

Broadening of Cyclotron Resonance Conditions in the Relativistic Interaction of an Intense Laser with Overdense Plasmas

Takayoshi Sano,^{1,*} Yuki Tanaka,¹ Natsumi Iwata,¹ Masayasu Hata,¹
Kunioki Mima,^{1,2} Masakatsu Murakami,¹ and Yasuhiko Sentoku¹

¹*Institute of Laser Engineering, Osaka University, Suita, Osaka 565-0871, Japan*

²*The Graduate School for the Creation of New Photonics Industries, Hamamatsu, Shizuoka 431-1202, Japan*

(Dated: August 28, 2018)

The interaction of dense plasmas with an intense laser under a strong external magnetic field has been investigated. When the cyclotron frequency for the ambient magnetic field is higher than the laser frequency, the laser's electromagnetic field is converted to the whistler mode that propagates along the field line. Because of the nature of the whistler wave, the laser light penetrates into dense plasmas with no cutoff density, and produces superthermal electrons through cyclotron resonance. It is found that the cyclotron resonance absorption occurs effectively under the broadened conditions, or a wider range of the external field, which is caused by the presence of relativistic electrons accelerated by the laser field. The upper limit of the ambient field for the resonance increases in proportion to the square root of the relativistic laser intensity. The propagation of a large-amplitude whistler wave could raise the possibility for plasma heating and particle acceleration deep inside dense plasmas.

I. INTRODUCTION

Remarkable progress has been made in the generation of an extremely strong magnetic field over kilo Tesla by using high power lasers [1–5]. Laser plasma interaction in such a field condition is now attracting much attention [6–9]. Existence of a strong field affects the laser-generated high energy density plasmas by microscopic energy transport and turbulence [10, 11] as well as by macroscopic hydrodynamics and instabilities [12–15]. To understand those processes is quite important for the various applications such as particle acceleration [16], inertial confinement fusion (ICF) [17–20], and laboratory laser astrophysics [21].

In this work, we focus on the propagation of a whistler wave in overdense plasmas. The electron cyclotron frequency ω_{ce} for a kilo-Tesla field becomes comparable to the laser frequency ω_0 . Here the critical field strength, of which the cyclotron frequency equals ω_0 , is defined as $B_c \equiv m_e \omega_0 / e \approx 10 (\lambda_0 / 1 \mu\text{m})^{-1}$ kT, where m_e is the electron rest mass, e is the elementary charge, and λ_0 is the laser wavelength. The laser light can enter overdense plasmas as a whistler wave when $\omega_{ce} > \omega_0$, because the cutoff frequency disappears. Furthermore, the whistler wave has another unique aspect that is the cyclotron resonance with electrons [22]. These features have a crucial meaning in laser plasma interaction, since the direct interaction between a high intensity laser and overdense plasmas could bring a new mechanism of efficient plasma heating and particle acceleration.

Electron acceleration associated with whistler waves have been studied in planetary magnetosphere plasmas [23–25]. It should be noted that the strong field ($\omega_{ce} > \omega_0$) and overdense ($\omega_{pe} > \omega_0$, where ω_{pe} is the plasma

frequency) situations we are considering here is also appropriate in the planetary plasmas. For example, in the Jovian magnetosphere, $\omega_{pe}/\omega_0 \sim 50$ and $\omega_{ce}/\omega_0 \sim 10$ for a kHz whistler mode [25]. However, the essential difference would be the whistler wave's amplitude when compared with the external field strength. For ultra-intense laser cases, the relativistic effects by the large-amplitude wave could make substantial changes in the wave propagation and energy conversion processes.

In this paper, we investigate the cyclotron resonance caused by an external magnetic field while taking into account the effects of relativistic electrons. Although the topic has been widely studied [26–28], our particular goal is to reveal the influence of the laser intensity on the resonance conditions for the field strength. Section II presents analytical consideration for the derivation of the resonance conditions in the interaction between an intense laser and magnetized overdense plasmas. The validity of the predicted conditions is confirmed numerically by a series of one-dimensional (1D) Particle-in-Cell (PIC) simulations of Sec. III. In Sec. IV, we will discuss the applications of the resonant properties of a ultra-intense laser under a strong magnetic field.

II. DERIVATION OF RESONANCE CONDITIONS

First, let us consider the cyclotron resonance condition for a right-hand (R) circularly polarized (CP) laser, that is, a large-amplitude whistler wave with a frequency ω_0 and a wavenumber k_0 . The relativistic Doppler-shifted cyclotron resonance condition is given by $\omega_0 - kv_{\parallel} = \omega_{ce}/\gamma$, where k and v_{\parallel} are the wavenumber and electron velocity along an external magnetic field B_{ext} of which the cyclotron frequency $\omega_{ce} = eB_{\text{ext}}/m_e$, and γ is the electron's Lorentz factor. Concentrating on

* sano@ile.osaka-u.ac.jp

a case where the wavenumber is identical to that of the incident whistler wave, $k = k_0$, the condition is rewritten as

$$\omega_0 \left(1 - \frac{\beta_{\parallel}}{\beta_{\phi}} \right) = \frac{\omega_{ce}}{\gamma}, \quad (1)$$

where $\beta_* \equiv v_*/c$ stands for the velocities normalized by the speed of light c , and $v_{\phi} = \omega_0/k_0$ is the phase velocity of the whistler mode. This relation contains two important factors which affect the resonance condition, namely the Doppler shift and relativistic effects.

The second term of left-hand side of Eq. (1) originates from the Doppler effect. The phase velocity v_{ϕ} of whistler waves in the electron density n_e can be much smaller than c ,

$$\beta_{\phi}^2 \approx \left(\frac{\omega_{pe}^2/\omega_0^2}{\omega_{ce}/\omega_0 - 1} \right)^{-1} \ll 1, \quad (2)$$

in strongly magnetized overdense plasmas ($\omega_0 < \omega_{ce} \ll \omega_{pe}$). Here, $\omega_{pe} = [e^2 n_e / (\varepsilon_0 m_e)]^{1/2}$ is the plasma frequency and ε_0 is the vacuum permittivity. The relativistic modification of dispersion relation for the whistler branch will only change by a small factor [29], so that this non-relativistic formula for v_{ϕ} may not affect the qualitative interpretation in the following discussion.

The resonant field strength is obtained as $\omega_{ce}/\omega_0 \approx 1 + (\beta_{\parallel} \omega_{pe}/\omega_0)^{2/3}$ from Eqs. (1) and (2) in the non-relativistic limit of $\gamma \approx 1$. The solution exists only for the electrons traveling in the opposite direction of the whistler wave, $v_{\parallel} v_{\phi} < 0$. This relation determines the resonant field strength as a function of the parallel velocity. Assuming v_{\parallel} is of the order of the thermal velocity v_{th} , it gives

$$\tilde{B}_{res} \approx 1 + \beta_{th}^{2/3} \tilde{n}_e^{1/3}, \quad (3)$$

where $\tilde{B}_* \equiv B_*/B_c$, $\tilde{n}_e \equiv n_e/n_c$, and $n_c = \varepsilon_0 m_e \omega_0^2 / e^2$ is the critical density. This condition indicates a small upper shift of the resonant field B_{res} from the critical value B_c , of which the cyclotron frequency $\omega_{ce} = \omega_0$. For the underdense cases, $n_e \ll n_c$, there is no gap from B_c because of the fast phase velocity $v_{\phi} \sim c$.

The relativistic effect in Eq. (1) can alter the resonance condition much more significantly. After the laser interaction, the electrons in dense plasmas moves mostly perpendicular to the external field by gyration. Ignoring the parallel velocity $v_{\parallel} \ll c$, the resonance condition for γ is given by $\gamma_{res} \approx \omega_{ce}/\omega_0$, or

$$\gamma_{res} \approx \tilde{B}_{ext}. \quad (4)$$

On the other hand, the quiver energy accelerated by the electric field E_0 of the CP laser is about $\gamma_q = (1 + a_0^2)^{1/2}$, where $a_0 = eE_0/(m_e c \omega_0^2)$ is the normalized vector potential of the laser light and the intensity is given by $I_0 = \varepsilon_0 c E_0^2$.

Only the laser-accelerated electrons that have acquired a larger energy than γ_{res} can get a chance for the resonance, so that the required condition is expressed as $\gamma_q \gtrsim \gamma_{res}$. Therefore, together with Eq. (3), the upper limit of the resonant strength for B_{ext} is summarized as

$$\tilde{B}_{upper} \sim \max \left\{ 1 + \beta_{th}^{2/3} \tilde{n}_e^{1/3}, (1 + a_0^2)^{1/2} \right\}. \quad (5)$$

In the non-relativistic limit, the cyclotron resonance occurs only at the specific condition of $\tilde{B}_{ext} = 1$. However, it turns out that the resonant condition has a wider range when including the relativistic effect, which is stimulated by the large-amplitude whistler wave.

III. VALIDATION BY NUMERICAL SIMULATIONS

Next, we have tested this predicted condition, Eq. (5), by performing a series of 1D collisionless PIC simulations [30]. In this numerical experiment, the interaction between a femto-second laser and a solid-density foil is examined. A thin hydrogenic target with 1 μm thickness is irradiated by a Gaussian-shape laser with 30 fs duration at half maximum amplitude. The electron number density of the target is set to be constant $\tilde{n}_e = 151$ ($n_e = 2.63 \times 10^{23} \text{ cm}^{-3}$). For simplicity, the foil is in contact directly with the vacuum without any preplasma.

The laser is assumed to be a RCP light traveling in the x direction. The wavelength is 0.8 μm , so that the critical magnetic field of this pulse is $B_c = 13.4 \text{ kT}$. The main pulse reaches the target at $t \approx 60 \text{ fs}$, and the simulation runs until 1 ps. The laser intensity is varied from weakly relativistic of $I_0 = 10^{18}$ ($a_0 = 0.484$) to strongly relativistic 10^{21} W/cm^2 (15.3). Collisionless approximations would be appropriate in this regime [31], while the collisional absorption is dominant at the much lower intensity [8, 32]. A uniform external magnetic field B_{ext} is applied along the laser propagation direction, which is constant in time throughout the computation in 1D situation.

For the PIC scheme, the Debye length is adopted as the size of the cell, where the initial electron temperature is assumed to be $T_e = 0.5 \text{ keV}$ unless otherwise mentioned. The particle number per cell for both electrons and ions is initially not less than 100 in all runs. The computational domain is sufficiently large, so that no particle and no electromagnetic field can reach the boundaries during the simulations.

Figure 1(a) shows the typical time history of the kinetic energies of electrons \mathcal{E}_e and ions \mathcal{E}_i converted from the incident laser energy \mathcal{E}_0 . Each particle has the kinetic energy ϵ , and \mathcal{E}_e (\mathcal{E}_i) is the sum of all electrons (ions) in the simulation box. The initial parameters in this fiducial model are $B_{ext} = 50.1 \text{ kT}$ ($\tilde{B}_{ext} = 3.74$) and $I_0 = 10^{21} \text{ W/cm}^2$. During the interaction with the main pulse ($t \sim 60\text{-}90 \text{ fs}$), the electrons gain a large amount of kinetic energy, and then it is transferred to the ions

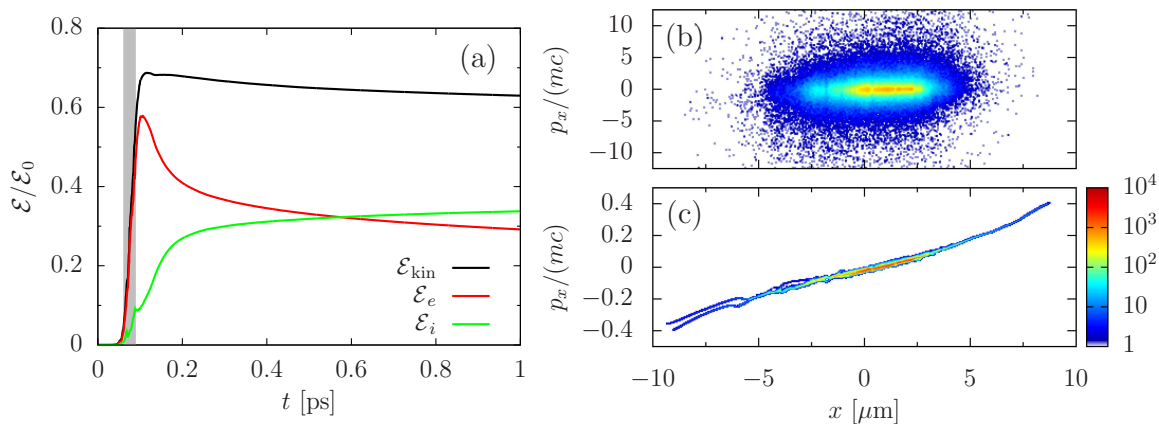


FIG. 1. (Color online) (a) Temporal evolution of plasma kinetic energies in the fiducial model for the electrons \mathcal{E}_e (red), ions \mathcal{E}_i (green), and total $\mathcal{E}_{\text{kin}} = \mathcal{E}_e + \mathcal{E}_i$ (black), which are normalized by the incident laser energy \mathcal{E}_0 . The gray area denotes the interaction duration of the laser with the plasma foil. (b,c) Phase diagram of the position x and momentum p_x for (b) the electrons and (c) ions, which are taken at the end of calculation $t = 1$ ps. The color shows the particle number. The initial location of the target foil is from $x = 0$ to $1 \mu\text{m}$.

gradually through the expansion process seen in Figs. 1(b) and 1(c). The total energy converted to electrons and ions reaches almost 70% of \mathcal{E}_0 , and which is one order of magnitude higher than that in the unmagnetized case ($\ll 10\%$).

Figure 2(a) depicts the energy absorption, which is the conversion efficiency from the laser to plasmas, evaluated at the end of calculations in various models with the different field strength B_{ext} and laser intensity I_0 . It is obvious that huge enhancement of the energy absorption takes place near the critical strength $B_{\text{ext}} \sim B_c$. If $\tilde{B}_{\text{ext}} \lesssim 0.1$, the external field makes little difference in the laser plasma interaction. Note that, for the lower intensity cases (e.g., $I_0 = 10^{18} \text{ W/cm}^2$), the peak is not exactly at B_c , but always shifted to a slightly larger strength due to the Doppler effect discussed above. The deviation estimated from Eq. (3) is $\tilde{B}_{\text{res}} \sim 1.7$ for this model, which is in good agreement with the numerical results.

When the laser intensity increases, the resonant absorption occurs with the wider range of B_{ext} . For the cases with $I_0 = 10^{21} \text{ W/cm}^2$, large absorption is achieved even when $\tilde{B}_{\text{ext}} \sim 10$. In order to check the ion contribution in the absorption process, simulations with immobile ions were performed which exhibits a similar trend to the cases with mobile ions [see open marks in Fig. 2(a)]. Therefore, we can conclude that the high absorption with the wider range of B_{ext} is caused by the cyclotron resonance of electrons with the relativistic effect inferred by Eq. (5).

It should be emphasized that the same conclusion is expected for the models with a linearly polarized (LP) laser [see Fig. 2(b)]. In dense plasmas, a LP light splits into left-hand (L) CP and RCP lights. Although the L wave part is reflected at the L cutoff ($\tilde{n}_e = 1 + \tilde{B}_{\text{ext}}$), the whistler part can propagate into and interact directly with the plasma. In fact, when the laser polarity in the

fiducial model switches to linear one, the acceleration by cyclotron resonance is still observed with the similar manner. But the fractional absorption becomes 33%, which is just half of the original CP model (63%).

To confirm the broadening of the cyclotron resonance, we can distinctly observe in Fig. 3 that the enhancement of the energy absorption is realized in the broader range of the external field B_{ext} with the increase of the normalized laser intensity a_0 . For a given a_0 , we have performed a number of simulations with different B_{ext} (e.g., Fig. 2) and have evaluated the upper and lower values of B_{ext} between which the absorption is above a threshold defined as $\Delta\mathcal{E}_{\text{kin}}/\mathcal{E}_0 = 0.1$. The numerically obtained B_{upper} traces the prediction curve given by Eq. (5) with a small scattering by factor of about 2. Note that the dependence of the upper limits on a_0 is unaffected qualitatively by the laser polarization and ion mobility, as demonstrated in Fig. 3. It might be better to estimate a_0 in this figure from the amplitude of the transmitted whistler wave, which becomes lower than that of the incident laser. But here, the difference is neglected for simplicity.

When the laser intensity is non-relativistic, $a_0 \lesssim 1$, the upper limits has little dependence on a_0 , and takes a constant value B_{res} which is influenced by the Doppler shift. If the intensity becomes relativistic, $a_0 \gtrsim 1$, the upper limits increase in proportion to a_0 because of the relativistic effects. On the other hand, the lower limits are always around B_c , unless the relativistic transparency comes into play as seen at $a_0 \sim 100$ [33, 34]. Thus the large conversion efficiency is induced at the broadened conditions of B_{ext} , which is shown by the gray region in Fig. 3.

Interestingly, the resonance process can be clearly identified in the velocity diagram of electrons. The resonance condition is expressed by using the parallel and perpen-

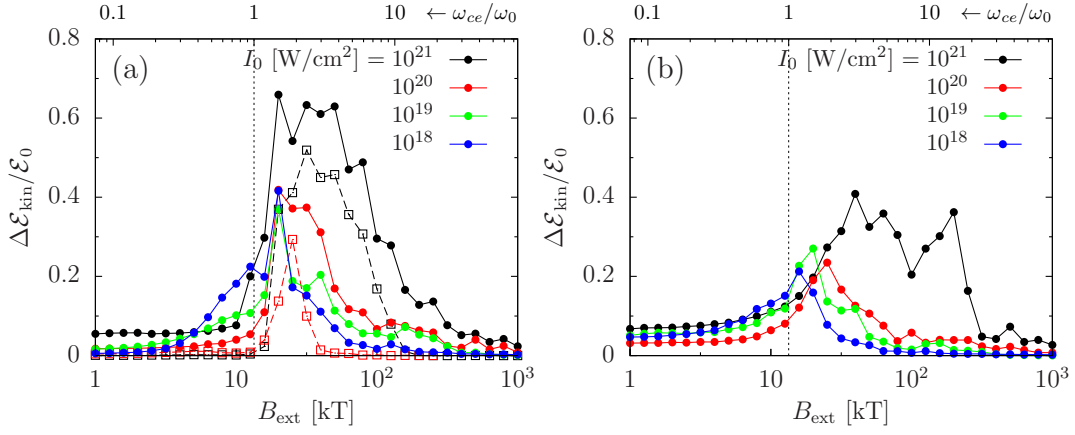


FIG. 2. (Color online) (a) Energy absorption evaluated by the gain of the total plasma energy $\Delta\mathcal{E}_{\text{kin}}$ as a function of the external field strength B_{ext} for the CP laser cases of $I_0 = 10^{21}$ (black), 10^{20} (red), 10^{19} (green), and 10^{18} W/cm² (blue). The critical field strength B_c is indicated by the dotted line. For the purpose of comparison, the results of the ion immobile runs for $I_0 = 10^{21}$ and 10^{20} W/cm² are also shown by the open squares. (b) The same figure as panel (a) for the LP laser cases.

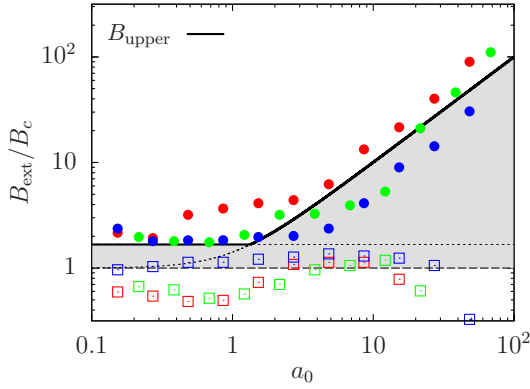


FIG. 3. (Color online) Upper limits of the external field strength B_{ext} (filled circles) for the range where the absorption rate is enhanced over a threshold value, which are shown as a function of the normalized intensity of the incident laser a_0 . The different colors indicate different model assumptions. The red and green marks are for the cases with the RCP and LP laser, respectively. The blue ones are with the RCP laser, but the ions are assumed to be immobile. The solid curve shows the theoretical prediction for \tilde{B}_{upper} given by Eq. (5) assuming $\tilde{B}_{\text{res}} = 1.7$. The lower limits obtained numerically are also plotted by the open squares.

dicular velocities, instead of γ , as

$$\beta_{\perp}^2 = 1 - \beta_{\parallel}^2 - \frac{1}{\tilde{B}_{\text{ext}}^2} \left(1 - \frac{\beta_{\parallel}}{\beta_{\phi}} \right)^2. \quad (6)$$

This condition for v_{\parallel} and v_{\perp} appears in the velocity diagram as two lines shown in Fig. 4 for the fiducial condition with $\tilde{B}_{\text{ext}} = 3.74$. Since the external field is much larger than B_c , there exists no resonant electrons at the beginning [Fig. 4(a)].

However, due to the penetration of a whistler wave, the resonance is triggered by relativistic electrons accelerated by the laser's electric field. During the laser interaction,

only the perpendicular velocity increases toward the relativistic regime, while v_{\parallel} is almost unchanged and keeps the thermal distribution [Fig. 4(b)]. When v_{\perp} hits the resonance condition at $\gamma \sim \gamma_{\text{res}}$ and $v_{\parallel} \sim 0$, further jump up of the electron energy starts through the cyclotron resonance. It is this resonance point indeed that is used in the derivation of γ_{res} [Eq. (4)].

The electron temperature is highly anisotropic at this phase ($T_{\perp} \gg T_{\parallel}$), so that the kinetic mirror instability could be driven [35, 36], resulting in the thermalization of the electrons. Then finally, high energy conversion is accomplished at the end of calculation [Fig. 4(c)].

By contrast, the resonant acceleration cannot happen if the laser intensity is lower. For a model with the intensity $I_0 = 10^{19}$ W/cm², the acceleration by the laser field is not enough to reach the resonance point because $\gamma_q < \gamma_{\text{res}}$ [Fig. 4(d)]. That is why there is no enhancement in the absorption efficiency.

Figure 4(e) shows the probability density function for the electron kinetic energy ϵ_e in the logarithmic binning $\epsilon f_{\epsilon}(\epsilon) = f_{\ln \epsilon}(\ln \epsilon)$. For the fiducial model, the quiver kinetic energy, $\epsilon_q = (\gamma_q - 1)m_e c^2$, can reach the requirement for the resonance $\gamma_{\text{res}} - 1 \approx 2.7$ or $\epsilon_e \approx 1.4$ MeV around the timing of $t = 0.05$ ps. Immediately after that, the maximum energy increases suddenly over 100 MeV by the resonant acceleration, which is much larger than the free-electron ponderomotive limit $\epsilon_p = m_e c^2 a_0^2 / 2 \approx 60$ MeV [37]. This could be happen only when the laser intensity satisfies $a_0 \gtrsim \gamma_{\text{res}}$. The electron heating in the $I_0 = 10^{19}$ W/cm² run is not by much and the energy of hot-electron component is at most the quiver kinetic energy $\epsilon_q \approx 0.93$ MeV.

Now, we will carefully inspect the trajectories of some representative electrons in the fiducial run throughout the laser plasma interaction from $t = 0$ to 150 fs. Figure 5(a) shows the time evolution of the kinetic energies of selected four particles. When the transmitted laser light is propagating inside of the foil as the whistler mode, the

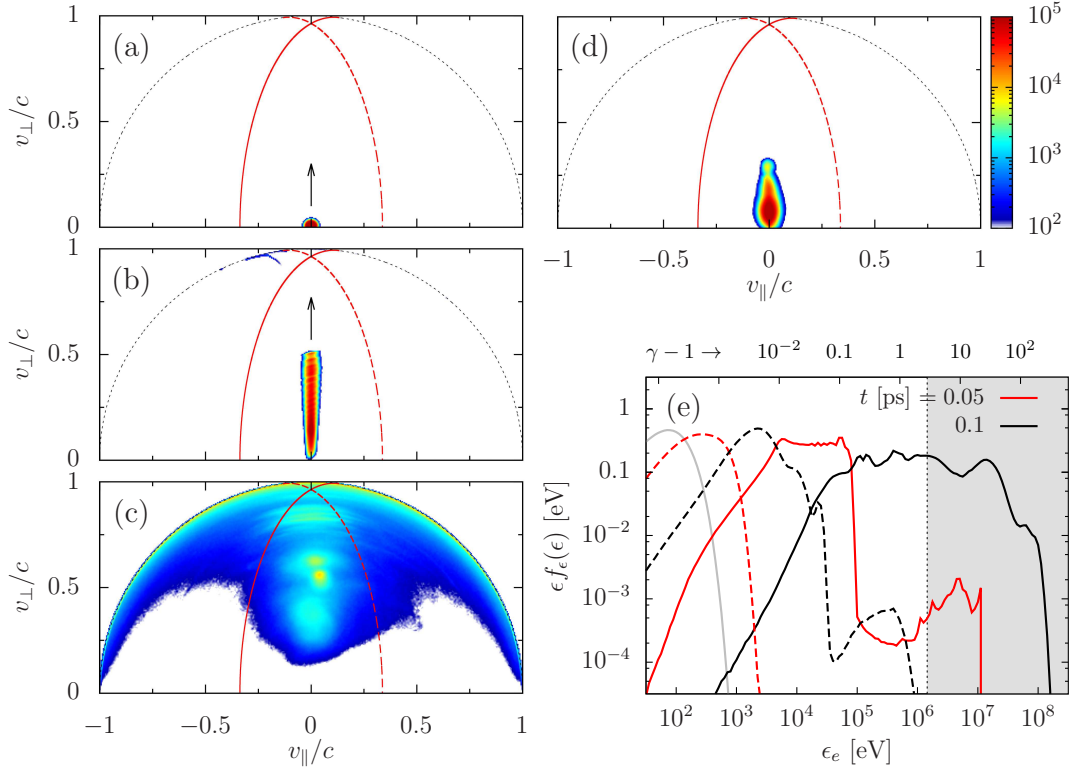


FIG. 4. (Color online) (a-c) Parallel and perpendicular velocity diagram of electrons, v_{\parallel} - v_{\perp} , for the fiducial model observed at (a) $t = 0$, (b) 0.05, and (c) 0.1 ps. The color denotes the particle number. The cyclotron resonance condition given by Eq. (6) is shown by the solid and dashed curves. The dotted curve denotes the upper limit of $|\mathbf{v}| = c$. (d) The same figure as panel (c) for a lower intensity $I_0 = 10^{19}$ W/cm\$^2\$. (e) Energy spectrum of electrons $\epsilon f_{\epsilon}(\epsilon)$ in the fiducial (solid) and lower intensity models (dashed) taken at $t = 0.05$ (red) and 0.1 ps (black). The gray curve is the initial Maxwellian spectrum of $T_e = 0.05$ keV. The resonance condition $\gamma \gtrsim \gamma_{\text{res}}$ is indicated by the gray zone.

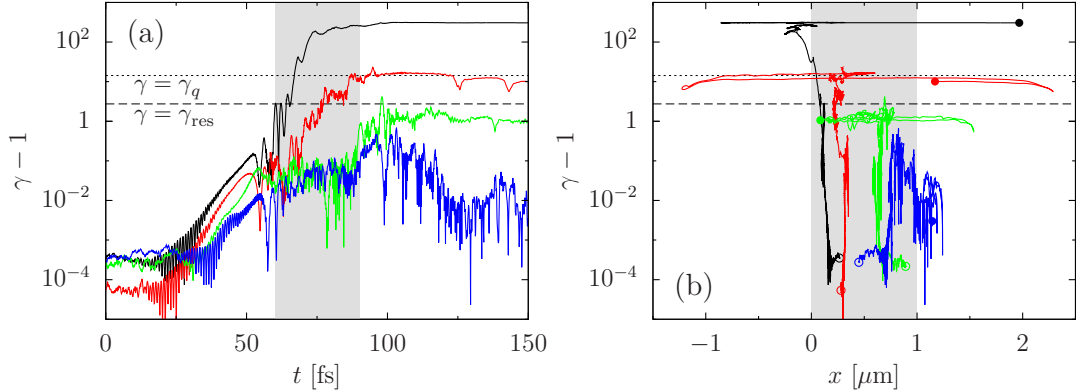


FIG. 5. (Color online) Trajectories of four representative electrons in the fiducial model shown by (a) the time-energy and (b) position-energy diagrams. The same color in the both panels means the track of an identical particle, which is drawn from $t = 0$ [open circles in panel (b)] to 150 fs (filled circles). Gray areas denote (a) the duration of 30 fs when the laser pulse is hitting the foil target and (b) the initial target location of 1 μm thickness. As a reference, the resonance condition $\gamma = \gamma_{\text{res}}$ and the quiver energy $\gamma = \gamma_q$ are depicted by the horizontal dashed and dotted lines, respectively.

electrons gain the energy gradually. The perpendicular velocity is accelerated predominantly by the CP electric field of the whistler wave. The acceleration up to the quiver energy $\gamma = \gamma_q$ takes place at almost the same location, which corresponds to the upward track in the

position-energy diagram of Fig. 5(b).

When the peak energy of an electron is below the resonance condition $\gamma = \gamma_{\text{res}}$, it loses the energy finally after the laser pulse is finished. However, if an electron successfully gains the energy reaching $\gamma = \gamma_{\text{res}}$, it can be

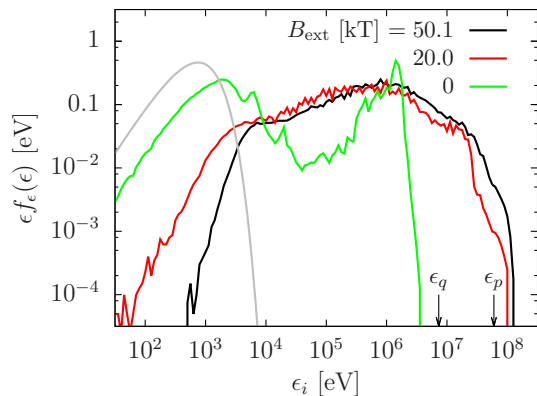


FIG. 6. (Color online) Energy spectrum of ions $\epsilon f_\epsilon(\epsilon)$ in the fiducial model (black) as well as the different B_{ext} runs with 20.0 kT (red) and nothing (green). The RCP laser with $I_0 = 10^{21}$ W/cm² is used in these models, and all the spectra are taken at $t = 1$ ps. The gray curve is the initial Maxwellian spectrum of $T_e = 0.5$ keV. The quiver kinetic energy of electrons ϵ_q and the free-electron ponderomotive limit ϵ_p are indicated by arrows.

kicked by the cyclotron resonance. Such electrons retain the gained energy (e.g., the 'red' trajectory in Fig. 5) and contribute the net absorption of the laser energy.

It is found that the acceleration beyond the free-electron ponderomotive limit ϵ_p commonly happens at just outside of the front surface of the target. All the superponderomotive electrons follow the exactly same track in Fig. 5(b) when the energy passes far over the quiver energy $\gamma = \gamma_q$. The incident laser is partly reflected at the surface, so that a CP standing wave is formed there. Direct acceleration by the static electric field of the standing wave would be the mechanism to generate such extreme electrons.

IV. DISCUSSION AND CONCLUSIONS

In summary, we have derived the relativistic condition of the cyclotron resonance for the interaction of overdense plasmas with an intense laser under a strong magnetic field. The condition is benchmarked successfully by 1D PIC simulations. The energy absorption increases dramatically when the external field strength is nearly equal to the critical value B_c . Furthermore, the cyclotron resonance operates at a wider parameter range when the laser is highly relativistic, $a_0 \gg 1$. In the models of a stronger field than B_c , the cyclotron resonance is allowed for the relativistic electrons only. On the other hand, the laser light propagates into overdense plasmas without cutoff for that cases. With a help of the intense laser field, such relativistic electrons are injected within the magnetized dense plasmas, and they trigger the efficient plasma heating via the broadened cyclotron resonance.

Ion acceleration is one of the potential applications [38, 39]. In this study, a large sheath potential is gen-

erated by hot electrons at the both target surfaces. The maximum ion energy increases through the target normal sheath acceleration (TNSA) [40] up to the comparable order of the superponderomotive electrons, $\epsilon_{i,\text{max}} \sim 100$ MeV. Since the TNSA is regarded as an energy conversion process from electrons to ions, the maximum ion energy could have some correlation with the electron energy [41]. Figure 6 shows the energy spectrum of ions for various B_{ext} cases. For the case of $B_{\text{ext}} = 0$, the maximum ion energy is of the order of the quiver kinetic energy of electrons, that is $\epsilon_q \approx 7.3$ MeV for this model. When the energy absorption by electrons is largely enhanced by the presence of a strong magnetic field, a significant fraction of ions is actually accelerated above the maximum energy in the unmagnetized run.

A good correlation between the maximum ion energy and the conversion efficiency can be seen in Fig. 7(a). This is also true for the LP laser cases, unless the $\mathbf{J} \times \mathbf{B}$ force becomes dominant at $B_{\text{ext}} \lesssim B_c$. For medical applications, heavy ion acceleration would be an interesting topic. When a 1 μm -thick carbon target with $\tilde{n}_e = 603$ (equivalent to the mass density of diamond $\rho = 3.51$ g/cm³) is irradiated by a LP laser with $I_0 = 10^{21}$ W/cm², the maximum energy is about 4 MeV/u at the range of $\tilde{B}_{\text{ext}} \sim 1\text{-}10$ [Fig. 7(b)]. Here, the wide resonance range of B_{ext} is the great advantage for the practical verification of this mechanism in future.

Direct plasma heating by electromagnetic waves might be attractive as an alternative scheme for the ICF. The systematic study of the propagation properties of whistler waves in dense plasmas should be a quite important next step. It is informative to extend the parameter space of the density and field strength, and make a chart like the Clemmow-Mullaly-Allis (CMA) diagram for the laser plasma interaction. Figure 8 is an example for the cases of the RCP laser with $I_0 = 10^{19}$ W/cm². The spots of high absorption trace the lines of the R cutoff and cyclotron resonance. Obviously the behavior of underdense plasmas is also affected by the external field, especially around $B_{\text{ext}} \sim B_c$. When $B_{\text{ext}} < B_c$, the laser light cannot enter the target if the density is higher than the R cutoff, and then it is mostly reflected at the surface.

In principle, the whistler waves can propagate into any density if $B_{\text{ext}} > B_c$, and deliver the energy directly to dense plasmas without going through hot electrons. This feature suggests a totally different way of the use of strong magnetic fields in the ICF plasmas from the previous work [17–20]. However the high absorption becomes an obstacle in terms of the propagation. In other words, the laser transmittance will be reduced by the amount of the energy absorption. The upper half of Fig. 8(a), where $B_{\text{ext}} > B_c$, shows that the energy absorption is larger when the density n_e is larger and B_{ext} is closer to B_c . But this feature disappears cleanly if the ion motion is inhibited, meaning that ion acoustic waves driven by the Brillouin instability [42] would play an important role for the high energy conversion there. The direct ion heating by whistler waves will be discussed in detail in

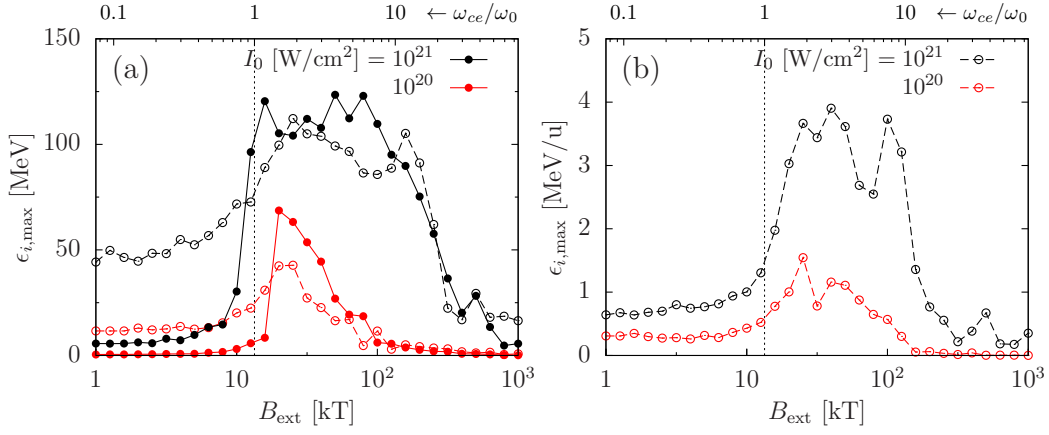


FIG. 7. (Color online) (a) Dependence of the external field strength B_{ext} on the maximum energy of ions $\epsilon_{i,\max}$ in the models of $I_0 = 10^{21}$ (black) and 10^{20} W/cm² (red). The LP laser cases are also shown by the open circles. The other parameters are identical to the models shown in Fig. 2. The dotted line indicates the critical field strength $\tilde{B}_{\text{ext}} = 1$. (b) The maximum ion energy for the models of a fully ionized carbon target. The LP laser is used and the other parameters are the identical to the fiducial hydrogen model.

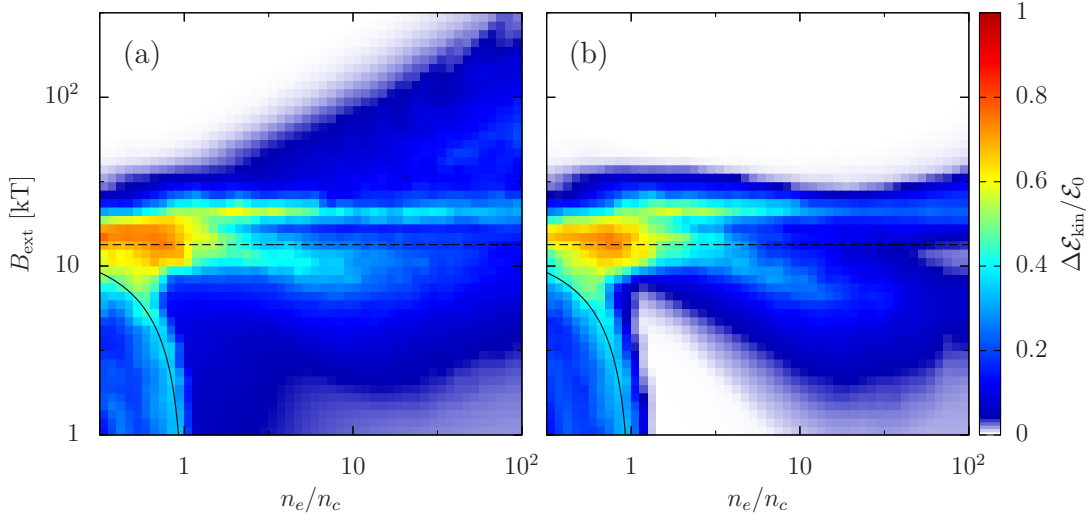


FIG. 8. (Color online) (a) Energy absorption in the density and field strength diagram constructed from the results of 50×50 simulations. The thickness of the hydrogen target is assumed to be $3 \mu\text{m}$ for these calculations. The RCP laser is used with the intensity $I_0 = 10^{19}$ W/cm². The solid and dashed lines denote the R cutoff ($\tilde{n}_e = 1 - \tilde{B}_{\text{ext}}$) and the cyclotron resonance ($\tilde{B}_{\text{ext}} = 1$), respectively. (b) The same figure as panel (a) for the immobile ion simulations.

the subsequent paper.

ACKNOWLEDGMENTS

We thank Y. Sakawa, S. Fujioka, A. Arefiev, and D. Kawahito for fruitful discussions and M. Zosa for his

careful reading of the manuscript. We also thank anonymous referees for their constructive comments. This work was supported by JSPS KAKENHI Grant Numbers JP26287147, JP15K21767, and JP16H02245. Computations were carried out on HCC at the Cybermedia Center and SX-ACE at the Institute of Laser Engineering of Osaka University.

[1] H. Yoneda, T. Namiki, A. Nishida, R. Kodama, Y. Sakawa, Y. Kuramitsu, T. Morita, K. Nishio, and T. Ide, Phys. Rev. Lett. **109**, 125004 (2012).

[2] S. Fujioka, Z. Zhang, K. Ishihara, K. Shigemori, Y. Hironaka, T. Johzaki, A. Sunahara, N. Yamamoto, H. Nakashima, T. Watanabe, H. Shiraga, H. Nishimura,

- and H. Azechi, *Sci. Rep.* **3**, 1170 (2013).
- [3] J. J. Santos, M. Bailly-Grandvaux, L. Giuffrida, P. Forestier-Colleoni, S. Fujioka, Z. Zhang, P. Korneev, R. Bouillaud, S. Dorard, D. Batani, M. Chevrot, J. Cross, R. Crowston, J.-L. Dubois, J. Gazave, G. Gregori, E. d'Humières, S. Hulin, K. Ishihara, S. Kojima, E. Loyez, J.-R. Marquès, A. Morace, P. Nicolai, O. Peyrusse, A. Poyé, D. Raffestin, J. Ribolzi, M. Roth, G. Schaumann, F. Serres, V. T. Tikhonchuk, P. Vacar, and N. Woolsey, *New J. Phys.* **17**, 083051 (2015).
- [4] P. Korneev, E. d'Humières, and V. Tikhonchuk, *Phys. Rev. E* **91**, 043107 (2015).
- [5] C. Goyon, B. B. Pollock, D. P. Turnbull, A. Hazi, L. Divol, W. A. Farmer, D. Haberberger, J. Javedani, A. J. Johnson, A. Kemp, M. C. Levy, B. Grant Logan, D. A. Mariscal, O. L. Landen, S. Patankar, J. S. Ross, A. M. Rubenchik, G. F. Swadling, G. J. Williams, S. Fujioka, K. F. F. Law, and J. D. Moody, *Phys. Rev. E* **95**, 033208 (2017).
- [6] X. H. Yang, W. Yu, H. Xu, M. Y. Yu, Z. Y. Ge, B. B. Xu, H. B. Zhuo, Y. Y. Ma, F. Q. Shao, and M. Borghesi, *Appl. Phys. Lett.* **106**, 224103 (2015).
- [7] W. Feng, J. Q. Li, and Y. Kishimoto, *Phys. Plasmas* **23**, 032102 (2016).
- [8] S. X. Luan, W. Yu, F. Y. Li, D. Wu, Z. M. Sheng, M. Y. Yu, and J. Zhang, *Phys. Rev. E* **94**, 053207 (2016).
- [9] J. X. Gong, L. H. Cao, K. Q. Pan, C. Z. Xiao, D. Wu, and X. T. He, *Phys. Plasmas* **24**, 033103 (2017).
- [10] S. I. Braginskii, *Rev. Plasma Phys.* **1**, 205 (1965).
- [11] A. A. Schekochihin, S. C. Cowley, S. F. Taylor, J. L. Maron, and J. C. McWilliams, *Astrophys. J.* **612**, 276 (2004).
- [12] T. Sano, T. Inoue, and K. Nishihara, *Phys. Rev. Lett.* **111**, 205001 (2013).
- [13] B. Albertazzi, A. Ciardi, M. Nakatsutsumi, T. Vinci, J. Béard, R. Bonito, J. Billette, M. Borghesi, Z. Burkley, S. N. Chen, T. E. Cowan, T. Herrmannsdörfer, D. P. Higginson, F. Kroll, S. A. Pikuz, K. Naughton, L. Romagnani, C. Riconda, G. Revet, R. Riquier, H.-P. Schlenvoigt, I. Y. Skobelev, A. Y. Faenov, A. Soloviev, M. Huarte-Espinosa, A. Frank, O. Portugall, H. Pépin, and J. Fuchs, *Science* **346**, 325 (2014).
- [14] H. Nagatomo, T. Johzaki, T. Asahina, A. Sunahara, T. Sano, H. Sakagami, K. Mima, S. Fujioka, H. Shiraga, and H. Azechi, *Nucl. Fusion* **55**, 093028 (2015).
- [15] K. Matsuo, H. Nagatomo, Z. Zhang, P. Nicolai, T. Sano, S. Sakata, S. Kojima, S. H. Lee, K. F. F. Law, Y. Arikawa, Y. Sakawa, T. Morita, Y. Kuramitsu, S. Fujioka, and H. Azechi, *Phys. Rev. E* **95**, 053204 (2017).
- [16] A. Arefiev, T. Toncian, and G. Fiksel, *New J. Phys.* **18**, 105011 (2016).
- [17] M. Hohenberger, P.-Y. Chang, G. Fiksel, J. P. Knauer, R. Betti, F. J. Marshall, D. D. Meyerhofer, F. H. Séguin, and R. D. Petrasso, *Phys. Plasmas* **19**, 056306 (2012).
- [18] L. J. Perkins, B. G. Logan, G. B. Zimmerman, and C. J. Werner, *Phys. Plasmas* **20**, 072708 (2013).
- [19] W.-M. Wang, P. Gibbon, Z.-M. Sheng, and Y.-T. Li, *Phys. Rev. Lett.* **114**, 015001 (2015).
- [20] S. Fujioka, Y. Arikawa, S. Kojima, T. Johzaki, H. Nagatomo, H. Sawada, S. H. Lee, T. Shiroto, N. Ohnishi, A. Morace, X. Vaisseau, S. Sakata, Y. Abe, K. Mat-
suo, K. F. F. Law, S. Tosaki, A. Yogo, K. Shigemori, Y. Hironaka, Z. Zhang, A. Sunahara, T. Ozaki, H. Sakagami, K. Mima, Y. Fujimoto, K. Yamanoi, T. Norimatsu, S. Tokita, Y. Nakata, J. Kawanaka, T. Jitsuno, N. Miyanaga, M. Nakai, H. Nishimura, H. Shiraga, K. Kondo, M. Bailly-Grandvaux, C. Bellei, J. J. Santos, and H. Azechi, *Phys. Plasmas* **23**, 056308 (2016).
- [21] B. A. Remington, R. P. Drake, and D. D. Ryutov, *Rev. Mod. Phys.* **78**, 755 (2006).
- [22] F. F. Chen, *Introduction to Plasma Physics and Controlled Fusion* (Plenum Press, New York, 1984).
- [23] Y. Omura, N. Furuya, and D. Summers, *J. Geophys. Res.* **112**, A06236 (2007).
- [24] D. Summers and Y. Omura, *Geophys. Res. Lett.* **34**, L24205 (2007).
- [25] R. B. Horne, R. M. Thorne, S. A. Glauert, J. Douglas Menietti, Y. Y. Shprits, and D. A. Gurnett, *Nat. Phys.* **4**, 301 (2008).
- [26] H. Liu, X. T. He, and S. G. Chen, *Phys. Rev. E* **69**, 066409 (2004).
- [27] V. S. Belyaev, V. P. Krainov, V. S. Lisitsa, and A. P. Matafonov, *Phys. Usp.* **51**, 793 (2008).
- [28] A. V. Arefiev, A. P. L. Robinson, and V. N. Khudik, *J. Plasma Phys.* **81**, 475810404 (2015).
- [29] V. I. Sotnikov, Y. Sentoku, and V. B. Krasovitskii, *Phys. Plasmas* **12**, 082107 (2005).
- [30] H. Matsumoto and Y. Omura, *Computer Space Plasma Physics* (Terra Sci., Tokyo, 1993).
- [31] A. J. Kemp, Y. Sentoku, V. Sotnikov, and S. C. Wilks, *Phys. Rev. Lett.* **97**, 235001 (2006).
- [32] D. F. Price, R. M. More, R. S. Walling, G. Guethlein, R. L. Shepherd, R. E. Stewart, and W. E. White, *Phys. Rev. Lett.* **75**, 252 (1995).
- [33] S. Palaniyappan, B. M. Hegelich, H.-C. Wu, D. Jung, D. C. Gautier, L. Yin, B. J. Albright, R. P. Johnson, T. Shimada, S. Letzring, D. T. Offermann, J. Ren, C. Huang, R. Hörlein, B. Dromey, J. C. Fernandez, and R. C. Shah, *Nature Phys.* **8**, 763 (2012).
- [34] D. J. Stark, T. Toncian, and A. V. Arefiev, *Phys. Rev. Lett.* **116**, 185003 (2016).
- [35] A. Hasegawa, *Plasma instabilities and nonlinear effects* (Springer-Verlag, Berlin, 1975).
- [36] D. B. Melrose, *Instabilities in space and laboratory plasmas* (Cambridge University Press, New York, 1986).
- [37] A. Sorokovikova, A. V. Arefiev, C. McGuffey, B. Qiao, A. P. L. Robinson, M. S. Wei, H. S. McLean, and F. N. Beg, *Phys. Rev. Lett.* **116**, 155001 (2016).
- [38] H. Daido, M. Nishiuchi, and A. S. Pirozhkov, *Rep. Prog. Phys.* **75**, 056401 (2012).
- [39] A. Macchi, M. Borghesi, and M. Passoni, *Rev. Mod. Phys.* **85**, 751 (2013).
- [40] S. C. Wilks, A. B. Langdon, T. E. Cowan, M. Roth, M. Singh, S. Hatchett, M. H. Key, D. Pennington, A. MacKinnon, and R. A. Snavely, *Phys. Plasmas* **8**, 542 (2001).
- [41] Y. Sentoku, T. E. Cowan, A. Kemp, and H. Ruhl, *Phys. Plasmas* **10**, 2009 (2003).
- [42] D. W. Forslund, J. M. Kindel, and E. L. Lindman, *Phys. Rev. Lett.* **29**, 249 (1972).